

Meta-Orbital Transition in Heavy-Fermion Systems: Analysis by Dynamical Mean Field Theory and Self-Consistent Renormalization Theory of Orbital Fluctuations

Kazumasa HATTORI

Institute for Solid State Physics, University of Tokyo, 5-1-5 Kashiwanoha, Kashiwa, Chiba 277-8581, Japan

We investigate a two-orbital Anderson lattice model with Ising orbital intersite exchange interactions on the basis of a dynamical mean field theory combined with the static mean field approximation of intersite orbital interactions. Focusing on Ce-based heavy-fermion compounds, we examine the orbital crossover between two orbital states, when the total f-electron number per site n_f is ~ 1 . We show that a “meta-orbital” transition, at which the occupancy of two orbitals changes steeply, occurs when the hybridization between the ground-state f-electron orbital and conduction electrons is smaller than that between the excited f-electron orbital and conduction electrons at low pressures. Near the meta-orbital critical end point, orbital fluctuations are enhanced and couple with charge fluctuations. A critical theory of meta-orbital fluctuations is also developed by applying the self-consistent renormalization theory of itinerant electron magnetism to orbital fluctuations. The critical end point, first-order transition, and crossover are described within Gaussian approximations of orbital fluctuations. We discuss the relevance of our results to CeAl_2 , CeCu_2Si_2 , CeCu_2Ge_2 , and related compounds, which all have low-lying crystalline-electric-field excited states.

KEYWORDS: dynamical mean field theory, two-orbital Anderson lattice model, self-consistent renormalization theory, critical end point, orbital fluctuations

1. Introduction

After the discovery of the unconventional superconductivity in CeCu_2Si_2 ,¹ various heavy-fermion compounds have attracted great attention. They exhibit many interesting phenomena,² such as quantum critical behaviors associated with the quantum critical point (QCP) of magnetic phase transitions under pressure, magnetic field and chemical substitutions, non-Fermi liquid properties near the QCP, and various types of unconventional superconductivity. It is expected that the Cooper pairs in such heavy-fermion superconductors are mediated by magnetic fluctuations, since the superconductivity always occurs near the magnetic phase.

Over the past ten years, the possible nonmagnetic-fluctuation-mediated superconductivity at high pressures separated from the superconductivity near the magnetic QCP has attracted much attention in some heavy-fermion compounds, such as CeCu_2Si_2 , CeCu_2Ge_2 , and related materials,^{3–7} since magnetic fluctuations are not developed there.⁸ Near the pressure where the superconducting transition temperature has a peak as a function of pressure, electric resistivity shows a linear temperature T dependence, with residual resistivity being enhanced.^{5–7} As pressure increases, Kadowaki-Woods ratio gradually varies from the value for strongly correlated systems to that for weakly correlated systems.⁹

To explain superconductivity without magnetic fluctuations, Onishi and Miyake¹⁰ proposed that Ce-valence fluctuations lead to unconventional superconductivity at high pressures in these systems on the basis of an extended periodic Anderson model (Ex-PAM). The ex-

istence of the valence transition in the Ex-PAM was confirmed by more elaborate numerical calculations later.^{11,12} The properties near the critical end point (CEP) of valence fluctuations explain the resistivity^{7,13} and changes in Kadowaki-Woods ratio.⁹

Experimentally, when the f-electron charge per site varies, owing to the electrostatic potential change around a Ce site, the lattice constant should also vary correspondingly, and some of the phonon branches should be affected by this change. However, no direct evidence for the steep changes in Ce valence has been reported.

In this paper, we will focus on the crystalline-electric-field (CEF), *i.e.*, orbital states in these systems. The materials mentioned above all have low-energy excited CEF states. CEF excitations are observed by inelastic neutron scattering experiments.^{14,15} Resistivity data also indicate the existence of excited CEF states, showing a two-peak structure as a function of temperature T . The two peaks correspond to two different Kondo temperatures. More importantly, the two peaks merge as pressure increases, and the pressure where the two peaks merge approximately coincides with the pressure where superconducting transition temperature increases as mentioned above.⁵ The two-peak structure and its variation as a function of pressure are well explained by the analysis of an orbital-degenerate Anderson lattice model.¹⁶ Interestingly, these behaviors are also observed in CeAl_2 , which is a prototype of heavy-fermion compounds, at around 3 GPa, while superconductivity has not been observed.¹⁷ A neutron scattering experiment revealed that there are also low-energy CEF states in CeAl_2 .¹⁸

Thus, it is natural to consider that the orbital (CEF) fluctuations in these systems play an important role in realizing the unconventional superconductivity at high pressures. In this paper, we will examine the orbital variations as a function of pressure on the basis of a dynamical mean field theory (DMFT)¹⁹ and show that a “meta-orbital” transition or crossover occurs when hybridizations between conduction and f-electrons depend on the orbital and are sufficiently small compared with the f-electron energy level. We also find that the orbital fluctuations couple with f-electron charge degrees of freedom, leading to the variation in f-electron occupancy when the orbital crossover or transition occurs. We will also try to construct an effective orbital fluctuation theory.

This paper is organized as follows. In §2, a two-orbital Anderson lattice model is analyzed on the basis of a dynamical mean field theory with Wilson’s numerical renormalization group method used as the impurity solver. A theory of critical fluctuations near the critical end point of orbital fluctuations is developed in §3 on the basis of the self-consistent renormalization theory. Finally, §4 shows the summary of the present paper.

2. Two-orbital Anderson Lattice Model with Ising Anisotropic Orbital Interaction

In this section, we investigate orbital fluctuations in a two-orbital Anderson lattice model with Ising orbital intersite exchange interactions on the basis of the DMFT¹⁹ combined with the static mean field approximation of intersite exchange interactions. As a solver for the effective impurity problem in the DMFT, we use Wilson’s numerical renormalization group (NRG) method, which is powerful for investigating zero-temperature properties of the impurity problem. We will show the zero-temperature properties of this system, including the variations in the orbital occupancy, the f-electron density of states, and the zero-temperature phase diagram.

2.1 Model

We investigate the periodic Anderson lattice model on a Bethe lattice with two localized f-orbitals ($\alpha = A$ or B) hybridizing with a single conduction electron band.¹⁶ We also include Ising orbital-orbital intersite interactions in our model and the Hamiltonian is given as

$$\begin{aligned}
 H = & \sum_{ij\sigma} (-t_{ij} - \mu\delta_{ij}) c_{i\sigma}^\dagger c_{j\sigma} + \sum_{i\alpha\sigma} [v_\alpha (c_{i\sigma}^\dagger f_{i\alpha\sigma} + \text{h.c.}) \\
 & + (\varepsilon_{f\alpha} - \mu) f_{i\alpha\sigma}^\dagger f_{i\alpha\sigma}] + \sum_{i\alpha} U_\alpha n_{if\alpha\uparrow} n_{if\alpha\downarrow} \\
 & + U' \sum_{i\sigma\sigma'} n_{ifA\sigma} n_{ifB\sigma'} - \frac{J_o^z}{z_{\text{n.n.}}} \sum_{\langle i,j \rangle} T_{iz} T_{jz}. \quad (1)
 \end{aligned}$$

Here, $c_{i\sigma}$ and $f_{i\alpha\sigma}$ represent the annihilation operators for conduction and f-electrons at site i , spin σ , and orbital α , respectively. The f-electron number and the orbital operator are defined as $n_{if\alpha\sigma} \equiv f_{i\alpha\sigma}^\dagger f_{i\alpha\sigma}$ and $T_{iz} \equiv \sum_\sigma (n_{ifA\sigma} - n_{ifB\sigma})$, respectively. J_o^z is the Ising

orbital interaction between the nearest neighbor sites, which is assumed as $J_o^z > 0$, and $z_{\text{n.n.}}$ is the number of nearest-neighbor sites. Since, in the DMFT, intersite correlations are neglected, we introduce this orbital interaction phenomenologically in order to take into account the correlations. Orbital interactions are generated by a fourth-order perturbation with respect to v_α , starting from the localized limit in a two-orbital Anderson lattice model, as shown in Appendix A. Hamiltonian (1) includes only one of the many interactions generated in fourth-order perturbations, such as spin-spin exchange and interactions between spin-orbital degrees. Since we are interested in the orbital fluctuations in a paramagnetic phase, we restrict ourselves to take into account the Ising orbital interaction in this paper. The notations used for other parameters are conventional.

Throughout this section, we set the nearest-neighbor hopping $t = 1/2$, which corresponds to half of the bandwidth $D = 2t = 1$, and we concentrate on analyzing zero-temperature $T = 0$ properties of Hamiltonian (1) and fix the total electron number per site $n = 1.8$, and $\varepsilon_{fA} = -0.5$ in the unit of D . As for the value of J_o^z , we will mainly discuss the case of $J_o^z = 0.02$ while briefly showing the results for $J_o^z = 0$ as a reference. Since we are interested in Ce-based heavy-fermion compounds, we analyze the f^1 configuration, *i.e.*, the configuration with $n_f \equiv \sum_{\alpha\sigma} n_{f\alpha\sigma} \simeq 1$. This is the reason why spin exchange interactions between A - and B - orbitals are absent in Hamiltonian (1), since they are irrelevant in the f^1 configuration. In the following, U_α and U' are set to be infinite in order to project out f^2 - f^4 configurations.

2.2 Analysis by the dynamical mean field theory

In the DMFT, a lattice model is mapped to an effective impurity one with an effective conduction electron bath.¹⁹ In our case, the effective impurity model is an impurity Anderson model with three localized orbitals hybridizing with single-band conduction electrons. In this paper, the intersite orbital interaction is approximated in the mean field level with a uniform amplitude. The effective impurity model is given as

$$\begin{aligned}
 H_{\text{eff}} = & \sum_{k\sigma} [\tilde{\epsilon}_k a_{k\sigma}^\dagger a_{k\sigma} + (\frac{\tilde{v}_k}{\sqrt{N}} a_{k\sigma}^\dagger c_\sigma + \text{h.c.})] - \mu \sum_\sigma c_\sigma^\dagger c_\sigma \\
 & + \sum_{\alpha\sigma} [v_\alpha (c_\sigma^\dagger f_{\alpha\sigma} + \text{h.c.}) + (\bar{\varepsilon}_{f\alpha} - \mu) f_{\alpha\sigma}^\dagger f_{\alpha\sigma}] \\
 & + \sum_\alpha U_\alpha n_{f\alpha\uparrow} n_{f\alpha\downarrow} + U' \sum_{\sigma\sigma'} n_{fA\sigma} n_{fB\sigma'}. \quad (2)
 \end{aligned}$$

Here, $\bar{\varepsilon}_{f\alpha}$ includes the contributions of the mean field value of T_{iz} : $\bar{\varepsilon}_{fA} = \varepsilon_{fA} - J_o^z \langle T_z \rangle$ and $\bar{\varepsilon}_{fB} = \varepsilon_{fB} + J_o^z \langle T_z \rangle$, where $\langle \dots \rangle$ indicates the expectation value and $\langle T_z \rangle = \langle T_{iz} \rangle$. The operators at the impurity site are defined as $f_{0\alpha\sigma} \equiv f_{\alpha\sigma}$ and $c_{0\sigma} \equiv c_\sigma$. The effective bath is represented by the bath conduction electron $a_{k\sigma}^\dagger$ hybridizing only with c_σ . The dispersion and hybridization of the bath conduction electrons are characterized by $\tilde{\epsilon}_k$ and

\tilde{v}_k , respectively, which are calculated self-consistently in the DMFT. Although one can integrate both $a_{k\sigma}$ and c_σ in a path-integral formulation, it is useful to employ the form (2) for NRG calculations.

To solve the impurity problem in the DMFT, we employ Wilson's NRG method,^{20,21} which is powerful for investigating the low-energy properties of the impurity problem. To calculate one-particle Green's functions correctly, we use the full-density-matrix NRG developed recently.^{22,23} In the Bethe lattice, the self-consistent equation of the DMFT reads

$$\Delta(\omega) = \frac{1}{N} \sum_k \frac{|\tilde{v}_k|^2}{\omega - \tilde{\epsilon}_k} = \frac{1}{4} G_c(\omega), \quad (3)$$

where $G_c(\omega) = -i \int_0^\infty dt e^{-i\omega t} \langle T \{ c_\sigma(t), c_\sigma^\dagger(0) \} \rangle$ being the local retarded Green's function for conduction electrons. In the NRG calculations in the DMFT self-consistent loops, we use the logarithmic discretization parameter $\Lambda = 1.8$ and mainly keep 300 low-energy states at each NRG iteration.²⁰ We also confirm that the results do not change when we increase the number of retained states up to 700.

2.2.1 Meta-orbital transition

In this subsection, we will show the numerical results of DMFT+NRG calculations. We will demonstrate that a meta-orbital transition and crossover occur in this system. We will also demonstrate that the orbital degrees of freedom couple with the f-electron charge ones.

Figure 1 shows the ε_{fB} dependence of orbital occupancy $\langle T_z \rangle$ for seven sets of v_B with fixed $v_A = 2v_B$. As ε_{fB} decreases, $\langle T_z \rangle$ decreases from ~ 1 to ~ -1 , indicating that the dominant orbital occupation changes from the A-orbital to the B-orbital. The variation in

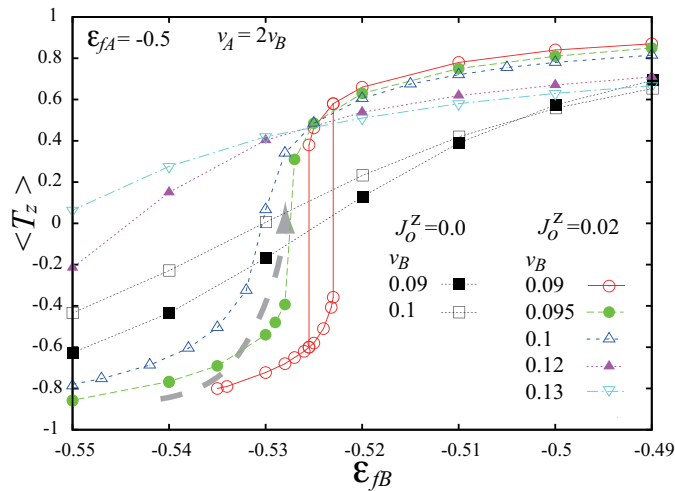


Fig. 1. (Color online) $\langle T_z \rangle$ vs ε_{fB} for several values of $v_B = 0.5v_A$, $\varepsilon_{fA} = -0.5$, and $J_o^z = 0.0$ and 0.02 , and the filling is fixed to be $n = 1.8$. The arrow indicates the typical variation in $\langle T_z \rangle$ for $J_o^z = 0.02$ as a function of pressure for Ce-based heavy-fermion systems.

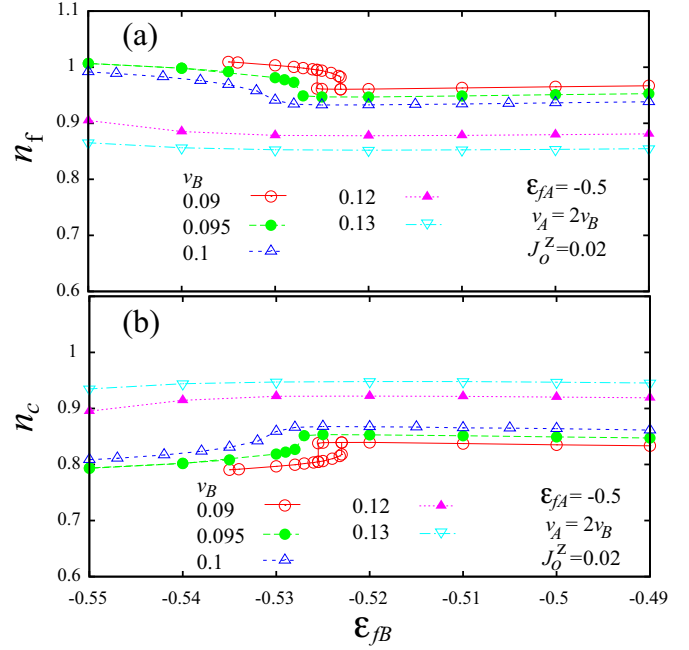


Fig. 2. (Color online) (a) n_f vs ε_{fB} and (b) n_c vs ε_{fB} for several values of $v_B = 0.5v_A$. The other parameters are the same as those in Fig. 1.

$\langle T_z \rangle$ as a function of ε_{fB} is gradual when $v_B (= 0.5v_A)$ is large, while it becomes steeper as v_B decreases. Finite J_o^z also enhances this steep change. Orbital occupancies for $J_o^z = 0.0$ with $v_B = 0.1$ (squares) and $v_B = 0.09$ (filled squares) change smoothly, while those for $J_o^z = 0.02$ with the same parameters show much steeper changes.

A CEP is located between $v_B = 0.095$ and 0.1 for $J_o^z = 0.02$. For $v_B = 0.09$, a first-order transition occurs. One can see a clear hysteresis, as shown in Fig. 1. For $v_B = 0.095$, although we have not detected a hysteresis in our calculation, it seems that there is a first-order transition.

These behaviors are analogues of meta-magnetism. In the present system, ε_{fB} and $\langle T_z \rangle$ correspond to the magnetic field and magnetization in the language of meta-magnetism, respectively. This meta-orbital transition is expected to occur in systems with several low-energy CEF states as the pressure increases. When the parameters are tuned, the CEP is realized. In Fig. 1, we also show the expected variations in v_B , ε_{fB} , and $\langle T_z \rangle$ in Ce-based compounds, with increasing pressure, indicated by an arrow for $J_o^z = 0.02$. Note that, as the pressure increases, both the hybridization and f-electron energy levels are expected to increase in Ce-based heavy-fermion compounds.

Figure 2 shows the ε_{fB} dependences of the total f-electron number n_f and the conduction electron number n_c with fixed $n = n_f + n_c = 1.8$. Note that, for $v_B \leq 0.1$, n_f is close to 1 for a small ε_{fB} , while $n_f \simeq 0.9-0.95$ for a large ε_{fB} . This is because $v_B < v_A$. When ε_{fB} is sufficiently small, for example, $\varepsilon_{fB} = -0.55$ and $v_B = 0.095$,

$\langle T_z \rangle \sim -0.9$, as shown in Fig. 1, which indicates that the f-electron occupies essentially the B -orbital. On the other hand, when ε_{fB} is large, the f-electron occupies mainly the A -orbital. In these two limiting cases, it is sufficient to consider a one-orbital Anderson lattice model. We obtain a low Kondo temperature T_K that leads to $n_f \sim 1$ for the small ε_{fB} with the relevant hybridization $v_B < v_A$, while a high T_K that leads to $n_f < 1$ for the large ε_{fB} with the relevant hybridization $v_A > v_B$.

As for the symmetry, the orbital, f-electron number, and conduction electron number belong to the same irreducible representation (scalar). Thus, as shown in Fig. 2, when the meta-orbital transition or crossover occurs, the f-electron number changes accordingly. We note that, across the transition and the crossover, the f-electron number is still close to 1, when v_A and v_B are not very large as expected in heavy-fermion systems. This point contrasts the results of the valence transition driven by the Coulomb repulsion between the f- and conduction electrons, U_{fc} , in the Ex-PAM, where a large variation in f-electron number occurs, owing to the large U_{fc} assumed.^{10–12}

2.2.2 Variation in density of states

Figure 3 shows the density of states (DOS) of f-electrons $-\text{Im}G_{fA,B}(\omega)/\pi$ for $v_B = 0.1 = 0.5v_A$ and several values of ε_{fB} . Here, $G_{fA(B)}(\omega)$ represents the local $A(B)$ -orbital f-electron retarded Green's function with the energy ω . In addition to the lower Hubbard-like peak located at the energy $\omega \sim \varepsilon_{fA,B} \sim -0.5$, there are several peaks in the low-energy region, reflecting the CEF excited states. The low-energy peak near $\omega \sim 0.2$ in the DOS of the B -orbital for $\varepsilon_{fB} = -0.44$ moves to a lower energy as ε_{fB} decreases, while a peak appears at a positive energy in the DOS of the A -orbital as ε_{fB} decreases, reflecting the meta-orbital crossover discussed previously. There is a sharp peak near $\omega = 0$ in $-\text{Im}G_{fA(B)}/\pi$. One can also see that there is a hybridization gap like structure for the $A(B)$ -orbital DOS when ε_{fB} is larger (smaller) than approximately $\varepsilon_{fB} \sim -0.53$, as shown in Figs. 3(b) and 3(c).

To investigate the low-energy DOS in more detail, we show the DOS at $\omega = 0$ as a function of ε_{fB} in Fig. 4, where we define $G_{\text{tot}} = G_{fA} + G_{fB} + G_c$. Since $\text{Im}G_c$ does not show notable changes, we do not show it. The DOS of the A -orbital at $\omega = 0$ is large when ε_{fB} is large, while it is small when ε_{fB} is small. Correspondingly, the DOS of the B -orbital at $\omega = 0$ is large for a small ε_{fB} and small for a large ε_{fB} . In Fig. 4, one can also see a clear hysteresis in the DOS at $\omega = 0$ for $v_B = 0.09$.

If we employ the variations in hybridization and f-electron level as pressure increases as shown by the arrow in Fig. 1, we observe that the DOS at the Fermi level decreases as pressure increases. The steepness of this variation depends on the distance to the CEP from the parameter path that corresponds to the physical pressure.

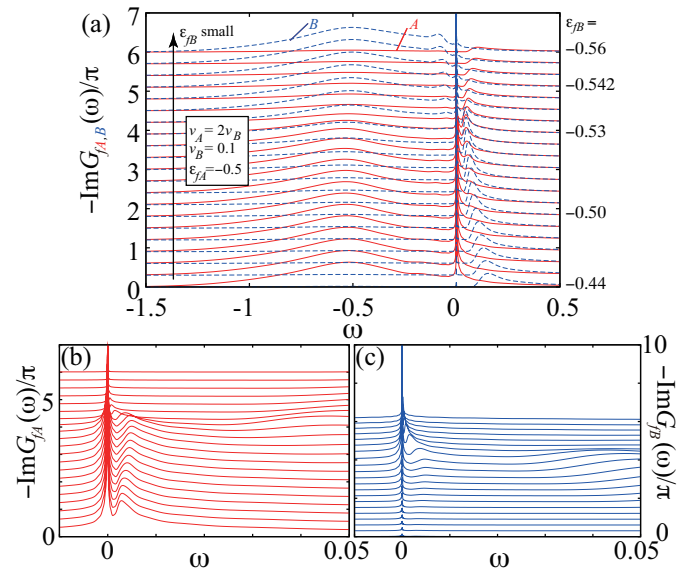


Fig. 3. (Color online) (a) f-electron density of states vs ω for $v_B = 0.1$ and $v_A = 0.2$ for several values of ε_{fB} . Full and dashed lines represent the DOS for the A - and B -orbitals, respectively. The values of ε_{fB} decrease from bottom to top as $\varepsilon_{fB} = -0.44, -0.45, -0.46, -0.47, -0.48, -0.49, -0.50, -0.505, -0.51, -0.515, -0.52, -0.525, -0.528, -0.53, -0.532, -0.535, -0.538, -0.542, -0.547, -0.555$, and -0.56 . Each line is shifted by 0.3. The other parameters are the same as those in Fig. 1. (b) Low-energy structure of A -orbital density of states. (c) Low-energy structure of B -orbital density of states.

2.2.3 Phase diagram

To summarize this section, we show the schematic ground state phase diagram of the two-orbital Anderson model with two different hybridizations ($v_B < v_A$) and ferro-orbital intersite interactions in Fig. 5. As discussed above, we observe a first-order transition line and its CEP. In Fig. 5, the “ $A(B)$ -rich” region indicates the region with a larger f-electron occupancy in the $A(B)$ -orbital. The “ A -rich” region is located in the larger ε_{fB} region, where the effective mass is smaller than that in the “ B -rich” region, owing to the large $v_A > v_B$. We also call it “light” Fermi liquid instead of heavy Fermi liquid. This light Fermi liquid can be regarded as the state with larger valence fluctuations than the B -rich state, since $v_A > v_B$. Near the CEP, f-electron charge fluctuations and also conduction electron ones are enhanced. The effective mass also changes steeply near the CEP, reflecting the variation in orbital occupancy.

Since our analysis is based on the DMFT and the mean field approximation for intersite orbital interactions J_o^z , we overestimate the effects of J_o^z . As shown in Fig. 1, the ε_{fB} dependence of $\langle T_z \rangle$ for $J_o^z = 0$ is much weaker than that for $J_o^z = 0.02$. We have not carried out DMFT+NRG calculations for a very small $v_B < 0.09$, since very small hybridizations make the NRG calculation difficult. When $J_o^z \rightarrow 0$, whether the first-order transition occurs or not is beyond the scope of the present

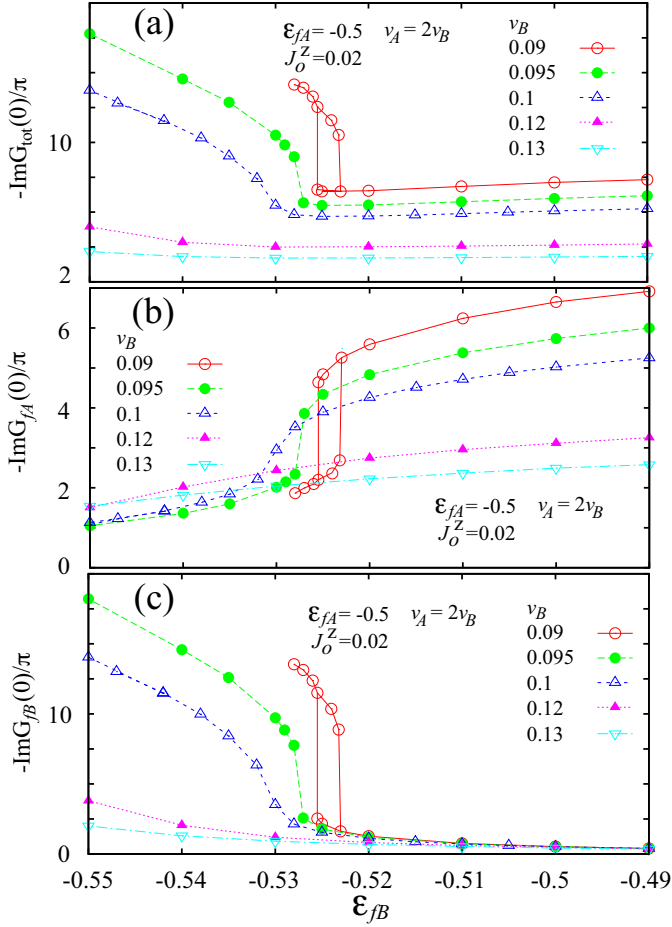


Fig. 4. (Color online) f-electron density of states at the Fermi level ($\omega = 0$) vs ε_{fB} . (a) Total density of states $-\text{Im}G_{\text{tot}}(0)/\pi$, (b) $-\text{Im}G_{fA}(0)/\pi$, and (c) $-\text{Im}G_{fB}(0)/\pi$. The other parameters are the same as those in Fig. 1.

analysis. However, it is noted that when one of the hybridizations is zero, there must be a first-order transition even when $J_o^z = 0$. To clarify whether this first-order transition exists in the region where the hybridization is finite, more elaborate numerical calculations that can take into account the intersite correlations are needed.

As for magnetic instabilities, it is expected that magnetic phases will appear in the phase diagram, especially in the region of the smaller v_B and ε_{fB} , corresponding to the low-pressure region in typical Ce-based heavy-fermion systems. Determining the phase diagram including the magnetic phases and their magnetic structures is beyond the scope of the present paper and we leave it as a future study. It is also interesting to investigate the case that the magnetic transition and the orbital CEP occur simultaneously. Such a situation might lead to a new universality class of magnetic phase transitions.

3. Self-Consistent Renormalization Theory of Nonmagnetic Orbital Fluctuations

In this section, we will develop a self-consistent renormalization theory for the orbital fluctuations discussed in

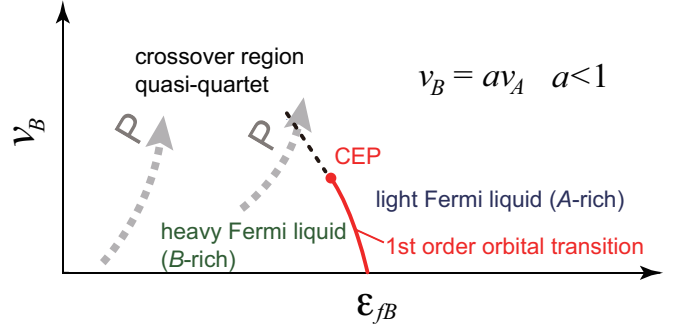


Fig. 5. (Color online) Schematic ground state phase diagram in v_B - ε_{fB} plane for $v_B = av_A$ with fixed constant $a < 1$. Arrows indicate examples of the parameter changes as the physical pressure P increases. The dotted line indicates the orbital crossover line where $\langle T_z \rangle \sim 0$. The critical end point is represented by a filled circle and the first-order transition line is indicated by a solid line. The hysteresis related to the first-order transition is not indicated. The left side of the first-order transition corresponds to the state with a larger effective mass due to the smaller hybridization v_B , while the right side of the first-order transition corresponds to that with a smaller effective mass, denoted as light Fermi liquid.

§2 on the basis of the DMFT. Since the DMFT does not take into account the long wavelength fluctuations, we use the one-loop self-consistent approximation scheme of the fluctuations known as the self-consistent renormalization (SCR) theory developed by Moriya and Kawabata for itinerant electron magnetism.^{24–26} When we apply the SCR theory to the nonmagnetic orbital fluctuations, we need to take into account the temperature dependence of the order parameter itself and the temperature dependence *originating from the order parameter in the mode-coupling corrections*. Our discussion in this section leads to results similar to those of the SCR theory for meta-magnetic fluctuations²⁷ and Kondo-volume-collapse transition in heavy-fermion systems.²⁸ It is noted that our formulation naturally describes both the order parameter and the mode-coupling corrections in an equal footing based on a variational principle. We will discuss the orbital fluctuations in three-dimensional ($d = 3$) systems in this paper, although the application to the cases with $d \neq 3$ is straightforward.

3.1 Landau-Ginzburg-Wilson action

The Landau-Ginzburg-Wilson action for nonmagnetic fluctuations generally has odd order terms with respect to field variables, which is given as

$$S = \sqrt{\frac{N}{T}} h \phi_0 + \frac{1}{2} \sum_p a_p \phi_p \phi_{-p} + b \sqrt{\frac{T}{N}} \sum_{p_1 p_2} \phi_{p_1} \phi_{p_2} \phi_{-p_1-p_2}$$

$$+c\frac{T}{N}\sum_{p_1 p_2 p_3}\phi_{p_1}\phi_{p_2}\phi_{p_3}\phi_{-p_1-p_2-p_3}. \quad (4)$$

Here, ϕ_p is the nonmagnetic field with $\phi_p^* = \phi_{-p}$, and p represents the momentum and energy. N and T are the number of lattice sites and temperature, respectively. In terms of S , the free energy F is given by $\exp(-F/T) = \int \mathcal{D}\phi \exp(-S)$. We neglect the momentum and energy dependence of the coefficients b and c , which are irrelevant from simple power counting in the context of the renormalization group. For the stability of the system, $c > 0$. h is the field conjugate to the uniform nonmagnetic field ϕ_0 ; thus, does not depend on p . Since we are interested in the orbital transition without breaking translational symmetry, we use the Ornstein-Zernike form of a_p as in the ferromagnetic fluctuation:^{24–26}

$$a_p = a_0 + A|\mathbf{q}|^2 + C|\omega_n|/|\mathbf{q}|, \quad (5)$$

where \mathbf{q} and ω_n are the momentum and the Bosonic Matsubara frequency, respectively. Existence of the odd order terms in eq. (4) leads to the first-order transition, CEP, and also crossover, as shown in Fig. 5.

3.2 Modified SCR theory

In the SCR theory, the non-Gaussian terms in the free energy F are approximated by mean field decoupling.^{24–26,29} This approximation corresponds to variationally determining the coefficients of the Gaussian fluctuations. In our case with the presence of h and b terms, we need to take into account the order parameter itself in addition to mode-coupling terms. We will show that a modified Gaussian action can describe the first-order transition, the CEP, and the crossover.

To describe the order parameter variations within the Gaussian approximation, we assume the following variational action:

$$S_{\text{eff}} = \frac{1}{2}\sum_{p \neq 0} r_p \phi_p \phi_{-p} + \sqrt{\frac{N}{T}} \tilde{h} \phi_0 + \frac{1}{2} r_0 \phi_0^2, \quad (6)$$

$$r_p = a_p + \delta, \quad (7)$$

where δ and \tilde{h} are variational parameters. On the basis of Gibbs-Bogoliubov-Feynman inequality, they are determined by minimizing $\bar{\Omega}$:³⁰

$$\bar{\Omega} \equiv \Omega_{\text{eff}} + T\langle S - S_{\text{eff}} \rangle, \quad (8)$$

$$\Omega_{\text{eff}} \equiv -T \log Z_{\text{eff}}, \quad (9)$$

$$Z_{\text{eff}} \equiv \int \mathcal{D}\phi \exp(-S_{\text{eff}}), \quad (10)$$

$$= \left(\prod_p \frac{1}{\sqrt{r_p}} \right) \exp\left(\frac{N}{T} \frac{\tilde{h}^2}{2r_0} \right), \quad (11)$$

$$\langle S \rangle \equiv \int \mathcal{D}\phi S \exp(-S_{\text{eff}})/Z_{\text{eff}}. \quad (12)$$

Defining the order parameter ϕ as $\phi = \sqrt{T/N} \phi_0$, we

obtain

$$\begin{aligned} \frac{\bar{\Omega}}{N} &= \frac{\Omega_{\text{eff}}}{N} + (h - \tilde{h})\langle \phi \rangle - \frac{\delta}{2}\langle \phi^2 \rangle + b\langle \phi^3 \rangle + c\langle \phi^4 \rangle \\ &+ 3(b\langle \phi \rangle + 2c\langle \phi^2 \rangle) \frac{T}{N} \sum_{p \neq 0} \frac{1}{r_p} - \frac{\delta T}{2N} \sum_{p \neq 0} \frac{1}{r_p} \\ &+ 3c \left(\frac{T}{N} \sum_{p \neq 0} \frac{1}{r_p} \right)^2. \end{aligned} \quad (13)$$

Since the effective action S_{eff} is Gaussian, we can analytically calculate $\langle \phi^n \rangle$ with n being any integers, and they are given as

$$\langle \phi \rangle = -\frac{\tilde{h}}{r_0}, \quad (14)$$

$$\langle \phi^2 \rangle = \frac{T}{N} \frac{1}{r_0} + \frac{\tilde{h}^2}{r_0^2} = \frac{T}{N} \frac{1}{r_0} + \langle \phi \rangle^2, \quad (15)$$

$$\langle \phi^3 \rangle = -\frac{T}{N} \frac{3\tilde{h}}{r_0^2} - \frac{\tilde{h}^3}{r_0^3} = 3\langle \phi^2 \rangle \langle \phi \rangle - 2\langle \phi \rangle^3, \quad (16)$$

$$\langle \phi^4 \rangle = -\frac{T^2}{N^2} \frac{3}{r_0^2} + \frac{T}{N} \frac{6\tilde{h}^2}{r_0^3} + \frac{\tilde{h}^4}{r_0^4} = 3\langle \phi^2 \rangle^2 - 2\langle \phi \rangle^4. \quad (17)$$

Differentiating $\bar{\Omega}_{\text{eff}}$ with respect to δ , we obtain

$$\begin{aligned} &\left[h - \tilde{h} + 3b \frac{T}{N} \sum_{p \neq 0} \frac{1}{r_p} + 3b\langle \phi^2 \rangle - 8c\langle \phi \rangle^3 - 6b\langle \phi \rangle^2 \right] \frac{\partial \langle \phi \rangle}{\partial \delta} \\ &+ \left[-\frac{\delta}{2} + 6c \frac{T}{N} \sum_{p \neq 0} \frac{1}{r_p} + 3b\langle \phi \rangle + 6c\langle \phi^2 \rangle \right] \\ &\times \frac{\partial}{\partial \delta} \left[\langle \phi^2 \rangle + \frac{T}{N} \sum_{p \neq 0} \frac{1}{r_p} \right] = 0. \end{aligned} \quad (18)$$

Using eq. (15) and defining

$$X \equiv \frac{T}{N} \sum_p \frac{1}{r_p}, \quad (19)$$

we obtain

$$\begin{aligned} &\left[h - \tilde{h} + 3bX - 3b\langle \phi \rangle^2 - 8c\langle \phi \rangle^3 \right] \frac{\partial \langle \phi \rangle}{\partial \delta} \\ &+ \left[-\frac{\delta}{2} + 6cX + 3b\langle \phi \rangle + 6c\langle \phi \rangle^2 \right] \frac{\partial}{\partial \delta} \left[\langle \phi \rangle^2 + X \right] = 0. \end{aligned} \quad (20)$$

Note that when $h = \tilde{h} = b = \langle \phi \rangle = 0$, eq. (20) leads to the self-consistent equation

$$\delta = 12cX, \quad (21)$$

which coincides with the conventional expression.^{24,26} Similarly, differentiating $\bar{\Omega}_{\text{eff}}$ with respect to \tilde{h} leads to

$$\begin{aligned} &\left[h - \tilde{h} + 3bX - 3b\langle \phi \rangle^2 - 8c\langle \phi \rangle^3 \right] \frac{\partial \langle \phi \rangle}{\partial \tilde{h}} \\ &+ \left[-\frac{\delta}{2} + 6cX + 3b\langle \phi \rangle + 6c\langle \phi \rangle^2 \right] \frac{\partial}{\partial \tilde{h}} \langle \phi^2 \rangle = 0. \end{aligned} \quad (22)$$

Combining eqs. (20) and (22), we obtain

$$\tilde{h} = h + 3bX - 3b\langle\phi\rangle^2 - 8c\langle\phi\rangle^3, \quad (23)$$

$$\delta = 12cX + 6b\langle\phi\rangle + 12c\langle\phi\rangle^2. \quad (24)$$

Equations (23) and (24) are the self-consistent equations in our theory.

Now, we derive the equation of state for $\langle\phi\rangle$. Using eqs. (14), (23), and (24), the equation of state is derived as

$$h + 3bX + (a_0 + 12cX)\langle\phi\rangle + 3b\langle\phi\rangle^2 + 4c\langle\phi\rangle^3 = 0. \quad (25)$$

Parameterizing $\langle\phi\rangle$ as $\langle\phi\rangle = \delta\phi - b/(4c)$ for later purposes, eq. (25) is rewritten as

$$\left[h - \frac{a_0b}{4c} + \frac{2b^3}{(4c)^2}\right] + \left(a_0 - \frac{3b^2}{4c} + 12cX\right)\delta\phi + 4c\delta\phi^3 = 0. \quad (26)$$

Equation (26) is the basic equation used to determine the order parameter $\delta\phi$. Note that $\delta\phi$ appears only in the form of $\delta\phi^2$ in X from the definition of $\delta\phi$ and eq. (24), and the effect of fluctuations on h in eq. (25) is canceled out by the shift of $\phi \rightarrow \delta\phi - b/(4c)$. The fluctuation term appears only in the coefficient of $\delta\phi$ in eq. (26). This equation describes the first-order transition, the CEP, and also the crossover while taking into account the mode-coupling correction X within the Gaussian fluctuation theory. A similar equation of state was introduced in ref. 28, where the renormalization of h was neglected in eq. (25).

Figure 6 shows the temperature and h dependences of the order parameter $\delta\phi$. Here, the critical value a_{0c} is given by eq. (36) and the parameters T_0 , T_A , and x_c introduced in Appendix B are fixed as $T_0 = 20$ K, $T_A = 50$ K and $x_c = 300$. In Fig. 6(a), there is a first-order transition for $h/2T_A \sim 0.05749$ below $T/T_0 \sim 0.01$. In Fig. 6(b), the parameter a_0 is fixed as $a_0 = a_{0c}$; and thus, at zero temperature, the CEP is realized at $h \sim 0.05476$. In Figs. 6(c) and 6(d), there is no phase transition and $\delta\phi$ varies smoothly as functions of T and h .

3.3 Zero-temperature critical end point

In this subsection, we investigate the nonmagnetic orbital fluctuations near the zero-temperature CEP in detail. Details of the calculations are summarized in Appendix B.

Near the zero-temperature CEP, $r_0 \sim 0$, X in eq. (19) is expanded in terms of r_0 as

$$X = K_0 + K_1r_0 + \mathcal{K}(T), \quad (27)$$

with

$$\begin{aligned} r_0 &= a_0 + 12c[K_0 + K_1r_0 + \mathcal{K}(T)] - \frac{3b^2}{4c} + 12c\delta\phi^2, \\ &= \frac{1}{1 - 12cK_1} \left[a_0 - \frac{3b^2}{4c} + 12c\delta\phi^2 + 12c(K_0 + \mathcal{K}(T)) \right] \end{aligned}$$

and

$$K_0 > 0, \quad K_1 < 0, \quad \text{and} \quad \mathcal{K}(T) > 0. \quad (29)$$

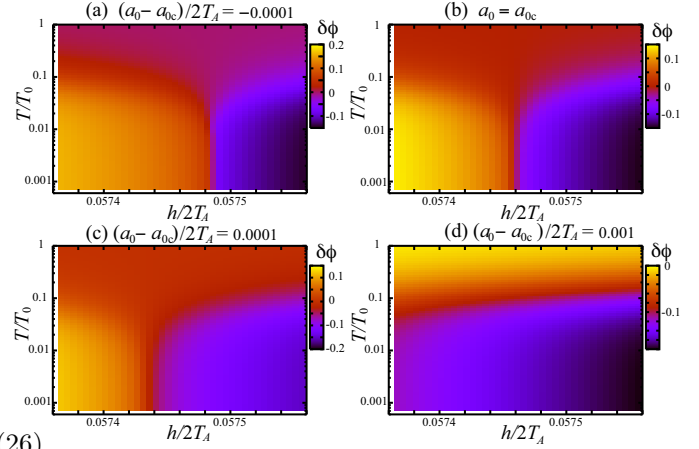


Fig. 6. (Color online) Contour plot of order parameter $\delta\phi$ in temperature- h plane for $b/2T_A = -0.01$, $c/2T_A = 0.01$, $T_0 = 20$ K, $T_A = 50$ K, and $x_c = 300$. (a) $(a_0 - a_{0c})/2T_A = -0.0001$, (b) $a_0 = a_{0c}$, (c) $(a_0 - a_{0c})/2T_A = 0.0001$, and (d) $(a_0 - a_{0c})/2T_A = 0.001$. In (a), a finite temperature critical end point appears at $h/2T_A \sim 0.05749$ and $T/T_0 \sim 0.01$, below which a first-order transition line exists. In (b), a zero-temperature critical end point exists at $h/2T_A \sim 0.05476$, where the order parameter $\delta\phi = 0$ for $T \geq 0$. In (c) and (d), changes in the order parameter are smooth, indicating the crossover.

As is well known, $\mathcal{K}(T) \propto T^{4/3}$ in three-dimensional systems with the dynamical exponent $z = 3$ ^{24,26} (see Appendix B). Now, substituting eqs. (27) and (28) into eq. (26), we obtain

$$H_0 + [A_0 + A_1\mathcal{K}(T)]\delta\phi + 4C_0\delta\phi^3 = 0, \quad (30)$$

where

$$H_0 = h - \frac{a_0b}{4c} + \frac{2b^3}{(4c)^2}, \quad (31)$$

$$A_0 = a_0 - \frac{3b^2}{4c} + \frac{12cK_1}{1 - 12cK_1} \left[a_0 - \frac{3b^2}{4c} + \frac{K_0}{K_1} \right] \quad (32)$$

$$A_1 = \frac{12c}{1 - 12cK_1} > 0, \quad (33)$$

$$4C_0 = 4c \left[1 + \frac{36cK_1}{1 - 12cK_1} \right]. \quad (34)$$

In the case that the $\delta\phi$ dependence of K_0 , K_1 , and $\mathcal{K}(T)$ is negligible, eq. (30) can be derived by minimizing the effective free energy F_{eff} given as

$$F_{\text{eff}} = H_0\delta\phi + \frac{1}{2}[A_0 + A_1\mathcal{K}(T)]\delta\phi^2 + C_0\delta\phi^4, \quad (35)$$

which is nothing but the Landau's free energy for ferromagnetism in the presence of the magnetic field $-H_0$.²⁷

Since $\mathcal{K}(T)$ vanishes at the zero-temperature CEP as $T^{4/3}$, the zero-temperature CEP is realized when $H_0 = A_0 = 0$, which is equivalent to $r_0 = 0$ and $\tilde{h} = 0$.²⁸ As a result, the critical value of the order parameter is $\delta\phi = 0$, leading to $\langle\phi\rangle_c = -b/(4c)$. In terms of the original parameters, we obtain the conditions for the zero-

temperature CEP as

$$a_{0c} = \frac{3b^2}{4c} - 12cK_0, \quad (36)$$

$$h_c = \frac{b^3}{(4c)^2} - 3bK_0, \quad (37)$$

at zero temperature. Using eqs. (36) and (37), eqs. (31) and (32) are rewritten as

$$H_0 = h - h_c, \quad (38)$$

$$A_0 = (a_0 - a_{0c}) \frac{1 + 12cK_1}{1 - 12cK_1}. \quad (39)$$

Let us discuss the temperature dependence of $\delta\phi$ near the zero-temperature CEP in the case of $C_0 > 0$ as expected for a small $c > 0$.

First, we consider the case that all the parameters, h , a_0 , b , c , A , and C are constant, *i.e.*, temperature-independent. Then, $H_0 = 0$ and $A_0 = 0$ in eq. (30), when the CEP is realized at zero temperature. We obtain $\delta\phi = 0$ or

$$\delta\phi^2 = -\frac{A_1(0)}{4C_0(0)}\mathcal{K}(T), \quad (40)$$

where $A_1(0)$ and $C_0(0)$ are the zero-temperature values of A_1 and C_0 , respectively. Since $A_1(0) > 0$, $\mathcal{K}(T) > 0$, and $C_0(0) > 0$, the solutions of eq. (40) are pure imaginaries. Thus, $\delta\phi = 0$ for all temperatures without taking into account the temperature dependence in the parameters. This corresponds to the order parameter variation in Fig. 6(b) for $h/2T_A \sim 0.05746$.

Secondly, we consider that the leading temperature dependence of the parameters is proportional to T^2 as expected in Fermi liquid states. In this case, eq. (30) becomes

$$A_1(0)\mathcal{K}(T)\delta\phi + 4C_0(0)\delta\phi^3 \simeq -H_0''T^2, \quad (41)$$

where $H_0 \simeq H_0''T^2$. Thus, we obtain $\delta\phi \propto T^{2/3}$, since this temperature dependence is self-consistent with $\mathcal{K}(T) \propto T^{4/3}$. Setting $\mathcal{K}(T) = \kappa T^{4/3}$ with $\kappa > 0$, and $\delta\phi = \varphi T^{2/3}$, we obtain

$$A_1(0)\kappa\varphi + 4C_0(0)\varphi^3 \simeq -H_0''. \quad (42)$$

When $A_1(0) > 0$ and $C_0(0) > 0$, eq. (42) always has only one solution φ , which is either positive or negative, depending on the sign of H_0'' . The first-order transition occurs as H'' changes for $A_1(0) < 0$ and $C_0(0) > 0$.

It is noted that ϕ couples any quantities and thus, in general, this nonanalytic temperature dependence $\delta\phi \propto T^{2/3}$ appears in any physical observables near the zero-temperature CEP. For example, the magnetic susceptibility χ_s has, rather than the usual T^2 dependence, the nonanalytic temperature dependence as

$$\chi_s^{-1}(T) \simeq \chi_s^{-1}(0) + \lambda\delta\phi + \dots \quad (43)$$

Here, λ is the coupling constant between magnetic and nonmagnetic fluctuations such as $\lambda\phi \sum_p M_p M_{-p}$ in the action, where M_p is the magnetic fluctuation at the mo-

mentum and the energy p . Thus, there might be a finite temperature region where $\chi_s(T) \propto T^{-2/3}$ is observed, when $\chi_s^{-1}(0)$ is suppressed by some factors. Since the present theory is phenomenological, the microscopic discussions on this issue are beyond the scope of this paper.

As for the other thermodynamic and transport quantities, we obtain the same critical behaviors as those in the ferromagnetic QCP with $z = 3$ and $d = 3$. The specific heat coefficient diverges as $C/T \sim -\log T$,³¹ and the resistivity is given as $\rho \sim T^{5/3}$,³² in the asymptotic limit. It is noted that, at a higher temperature, $\rho \propto T$ as is the case for all the bosonic fluctuations.

3.4 Critical end point at finite temperature

Here, we discuss the temperature dependence of $\delta\phi$ near a finite-temperature CEP at $T = T^* > 0$.

As in the case of the zero-temperature CEP discussed in §3.3, we first consider the case that all the parameters have no temperature dependence. In this case, $\delta\phi = 0$ for $T > T^*$ and $\delta\phi \propto \sqrt{\mathcal{K}(T^*) - \mathcal{K}(T)}$ for $T < T^*$. Thus, we obtain $\delta\phi \propto (T^* - T)^{1/2}$ near $T \sim T^*$, exhibiting the mean field behaviors. This is understood by noting that our theory is essentially mean field approximation and that the $H_0 = 0$ line in the parameter space corresponds to the case of the Ising model without magnetic fields, identifying $A_0 + A_1\mathcal{K}(T)$ as $T - T_c$, where T_c is the magnetic transition temperature.

In the second case, the temperature dependence of all the parameters is proportional to T^2 as derived in Fermi liquid states. Expanding the temperature dependence from the critical end point temperature T^* , we obtain

$$0 \simeq \left. \frac{\partial H_0}{\partial T} \right|_{T=T^*} (T - T^*) + 4C_0(T^*)\delta\phi^3. \quad (44)$$

Here, we assume $T^* \ll T_{FL}$, where T_{FL} is the so-called Fermi liquid temperature below which the Fermi liquid behaviors appear. In eq. (44), the temperature dependence in the second term in eq. (26) or (30) is on the higher order in $(T - T^*)/T^*$, and thus we neglect it. Then, the asymptotic temperature dependence of the order parameter $\delta\phi$ near the finite-temperature CEP is

$$\delta\phi = \pm \left| \frac{1}{4C_0(T^*)} \frac{\partial H_0}{\partial T} \right|_{T=T^*}^{\frac{1}{3}} |T^* - T|^{\frac{1}{3}}. \quad (45)$$

Comparing this with the result at the zero-temperature CEP as discussed in Sec. 3.3, one can see that there is a classical-quantum crossover from $\delta\phi \propto |T - T^*|^{1/3}$ to $\delta\phi \propto T^{2/3}$ as T^* decreases in the second case.

Physically, it is unrealistic to consider $H_0 = 0$ for all temperatures in real materials; thus, the second case is more realistic for experimental situations. However, the first case is pedagogically important, since it clearly exhibits this transition belonging to the Ising-type universality class as expected. It is also important to note that $\delta\phi \propto T^{2/3}$ is realized only when T_{FL} is well defined, *i.e.*,

when the Fermi liquid theory is valid and the condition $T/T_{FL} \ll 1$ is realized.

4. Discussion and Summary

We have discussed orbital fluctuations in a two-orbital Anderson lattice model on the basis of the DMFT in §2 and constructed a self-consistent critical theory of the orbital fluctuations in §3.

In the first part of this paper in §2, we have investigated meta-orbital transition in the two-orbital Anderson model with anisotropic intersite orbital-orbital interactions, and the schematic phase diagram is shown in Fig. 5 as the summary of §2.

First, our results demonstrate that a meta-orbital transition or crossover with steep changes in orbital occupancy occurs as pressure increases, only when the hybridization between the conduction electrons and the f-electrons at ambient pressure is sufficiently small. For simplicity, let us consider that the pressure affects the hybridizations only. Evidently, if the ambient pressure is located on the right side of the first-order transition line in Fig. 5, the meta-orbital transition and crossover do not occur as pressure increases, since v_B increases as pressure increases. On the other hand, if the ambient pressure is located on the left side of the first-order transition line, it is possible to realize them, and if the parameters are tuned, the CEP is realized. Here, we note that the f-electron ground state multiplet on the right side of the first-order transition line is the A -orbital, while it is the B -orbital on the left side of the line. Thus, it is concluded that the meta-orbital transition or crossover is realized only when the hybridization between the conduction electrons and the ground state multiplet of f-electrons at ambient pressure is *smaller* than that between the conduction electrons and the excited CEF multiplet. These observations are valid when the dominant effect of the pressure is the variation in $v_{A,B}$.

As far as we know, there is no compound that shows a first-order meta-orbital transition as pressure increases. This might indicate that the ferro-orbital interaction is small in the real materials or transverse orbital, and other interactions smear out the first-order transition. As mentioned in §2.2.3, it is important to clarify whether the first-order transition occurs in the model without J_o^z . Since J_o^z has been phenomenologically introduced to incorporate the orbital-orbital interactions in the DMFT calculations, we need to investigate the $J_o^z = 0$ model on the basis of more elaborate methods that can take into account both the local and intersite interactions.

Another important result shown in §2 is that the meta-orbital transition or crossover affects the f-electron occupancy. As shown in Fig. 2, f-electron occupancy slightly changes, when the meta-orbital transition or crossover occurs. This is understood by noting the hybridizations $v_A \neq v_B$. This contrasts with the large valence change discussed in the context of the valence transition driven by the large Coulomb repulsion U_{fc} , where the f-electron

occupation number n_f cannot be close to 1, when the CEP is realized. The large U_{fc} also affects the conduction electrons. Our recent study of the Ex-PAM based on DMFT+NRG calculations reveals that, when the valence crossover occurs as pressure increases for the large U_{fc} comparable to the bandwidth, the resulting density of states of the conduction electrons near the crossover point shows a Hubbard-like peak deep below the Fermi level and a sharp peak near the Fermi level, which indicates the existence of strongly correlated conduction electrons.

In the second part of this paper in §3, we have developed a self-consistent renormalization theory of the orbital fluctuations. There, we have paid special attention to the order parameter dependence of the mode-coupling term and derived self-consistent equations, which lead to an equation of state for the order parameter. We have succeeded in describing the first-order transition and crossover including the CEP of the orbital fluctuations. The temperature dependence of the order parameter $\propto T^{2/3}$ is consistent with that in the Kondo-volume-collapse theory²⁸ and possibly consistent with that in the valence transition,³³ since the symmetries of these order parameters are the same.

As for the temperature dependence of the resistivity, it is shown⁷ that the valence fluctuations lead to the T -linear dependence near the CEP, assuming a small A in eq. (5) from the results of the slave boson theory.¹⁰ It is noted that the T -linear temperature dependence is realized in all the bosonic fluctuations at high temperatures. For example, phonon scatterings lead to such a behavior at high temperatures. In the case of the orbital fluctuations, it is not clear whether the A coefficient in eq. (5) is sufficiently small in the present analysis. The precise determination of the A coefficient needs a more quantitative analysis. When $A \sim 0$ in eq. (5), we obtain $\mathcal{K}(T) \propto T^{2/3}$ near the CEP³³ and the equation of state (30) leads to $\delta\phi \propto T^{4/3}$ when all the parameters vary as a function of T^2 at low temperatures. Note that this temperature dependence should be cut off at the scale T_A , below which the asymptotic behaviors characteristic to $d = 3$ and $z = 3$ discussed above appear.

In our theory, it is expected that CeCu_2Si_2 and related compounds and CeAl_2 at ambient pressure are on the left side of the line of the first-order transition in Fig. 5, *i.e.*, in the B -rich phase. As for superconductivity, it is expected that compounds that show superconductivity away from their magnetic QCP pass near the CEP in Fig. 5 as pressure increases, while nonsuperconducting materials, such as CeAl_2 , are not sufficiently close to the CEP, assuming that magnetic phases exist on the left side in the phase diagram in Fig. 5. Since there are many aspects that affect the realization of superconductivity, such as the energy scale of the fluctuations and band structures,³⁴ more quantitative model and analysis are needed in order to clarify the details of the superconductivity realized in these systems.

In summary, we have investigated orbital fluctuations in heavy-fermion systems. We have shown that a meta-orbital transition occurs as pressure increases and the orbital variations affect the density of states at the Fermi level and also f-electron occupancy. We have also constructed an effective critical theory for the orbital fluctuations, which describes both the first-order transition and crossover on the basis of a variational principle. Our results give a possible scenario for the superconductivity and non-Fermi liquid behaviors associated with orbital fluctuations in heavy-fermion systems.

Acknowledgment

The author would thank H. Tsunetsugu, K. Miyake, and Y. Nishida for useful discussions. This work was supported by a Grant-in-Aid for Scientific Research (No. 20740189) from the Japan Society for the Promotion of Science.

Appendix A: Localized limit and intersite interactions

In this appendix, we will derive the intersite orbital interaction via a fourth-order perturbation in v_α from the localized limit of the Hamiltonian (1) without the J_o^z term. Note that J_o^z is not exactly the same as the orbital intersite interaction that will be derived in this appendix. J_o^z has been introduced phenomenologically in order to take into account the intersite orbital correlation in the DMFT calculation in §2.

Let us consider Hamiltonian (1) without J_o^z . In the limit of $U_\alpha, U' \rightarrow \infty$, and $\varepsilon_{f\alpha} \rightarrow -\infty$ keeping $U_\alpha/|\varepsilon_{f\beta}| \gg 1$ and $v_\alpha v_\beta/\varepsilon_{f\gamma}$ finite, the local excited configuration of f^0 contributes to the low-energy properties of this system only as virtual states and configurations with $f^n (n \geq 2)$ are neglected. Thus, the effective Hamiltonian can be written by the localized spin and orbital degrees of freedom interacting with conduction electrons via exchange interactions:

$$\begin{aligned} H_{\text{ex}} = & \sum_{ij\sigma} (-t_{ij} - \mu\delta_{ij}) c_{i\sigma}^\dagger c_{j\sigma} + \sum_{i\alpha\sigma\sigma'} J_\alpha c_{i\sigma}^\dagger(\mathbf{s}^c)_{\sigma\sigma'} c_{i\sigma'} \cdot \mathbf{S}_i \\ & + \Delta \sum_i T_{iz} + \sum_{i\sigma\sigma'} J_{AB} c_{i\sigma}^\dagger(\mathbf{s}^c)_{\sigma\sigma'} c_{i\sigma'} T_{ix} \cdot \mathbf{S}_i \\ & + K_{AB}^z \sum_i n_{ic} T_{iz} + K_{AB}^\pm \sum_i n_{ic} T_{ix}, \end{aligned}$$

where \mathbf{S}_i represents the f-electron spin operator at site i and the conduction electron spin is given as $s_\mu^c = \sigma_\mu/2$, where σ_μ with $\mu = x, y$ or z is the Pauli matrix. n_{ic} is the conduction electron charge operator $n_{ic} = \sum_\sigma c_{i\sigma}^\dagger c_{i\sigma}$. As for the orbital degrees of freedom of f-electrons, $T_{ix} = \sigma_x$ and $T_{iz} = \sigma_z$ acting on the orbital space at site i and the two eigenvalues of T_{iz} are 1 for the A -orbital and -1 for the B -orbital. The coupling constants are given as

$$J_\alpha = \frac{v_\alpha^2}{-\varepsilon_f}, \quad (\text{A.2})$$

$$J_{AB} = 4K_{AB}^\pm = \frac{2v_A v_B}{-\varepsilon_f}, \quad (\text{A.3})$$

$$K_{AB}^z = \frac{v_A^2 - v_B^2}{-4\varepsilon_f}. \quad (\text{A.4})$$

Here, we assume $\varepsilon_{fA} \sim \varepsilon_{fB} \equiv \varepsilon_f$ and ignore the difference between ε_{fA} and ε_{fB} in the denominator of J_α , J_{AB} , K_{AB}^z , and K_{AB}^\pm . The difference is taken into account in $\Delta = \varepsilon_{fA} - \varepsilon_{fB}$.

Now, intersite interactions in the second-order perturbations of J_α , J_{AB} , K_{AB}^z , and K_{AB}^\pm are obtained straightforwardly. Among them, the Ising-type orbital-orbital interaction is given as

$$K_{AB}^z \sum_{i,j} T_{iz} \chi_{ij}^c T_{jz}, \quad (\text{A.5})$$

where χ_{ij}^c is the conduction electron charge susceptibility. Note that, when $v_B \gg v_A$ (or $v_A \gg v_B$), the coupling constant J_B (or J_A) and $|K_{AB}^z|$ is much larger than J_{AB} and K_{AB}^\pm . In this limit, the spin-spin and Ising orbital interactions on the fourth order in v_α are more important than those in the other sectors, such as the transverse orbital and spin-orbital coupled interactions.

Appendix B: Detailed calculations in SCR theory

In this appendix, we summarize the detailed calculations of the mode coupling correction X in the SCR theory in order to make this paper self-contained.

Let us parameterize X in eq. (19) as

$$X = \frac{T}{N} \sum_{\mathbf{q}, n} \frac{1}{r_0 + A|\mathbf{q}|^2 + C|\omega_n||\mathbf{q}|^{-\theta}}, \quad (\text{B.1})$$

with $\theta = 1$. Following the discussions by Misawa *et al.*,²⁹ eq. (B.1) is reduced to

$$X = \mathcal{K}(0) + \mathcal{K}(T), \quad (\text{B.2})$$

$$\mathcal{K}(0) = \frac{K_d}{\pi} \int_0^{q_c} dq \int_0^\infty d\omega \frac{C\omega q^{d+\theta-1}}{[q^\theta(r_0 + Aq^2)]^2 + (C\omega)^2}, \quad (\text{B.3})$$

$$\mathcal{K}(T) = \frac{2K_d}{\pi} \int_0^{q_c} dq \int_0^\infty d\omega \frac{n_B(\omega) C\omega q^{d+\theta-1}}{[q^\theta(r_0 + Aq^2)]^2 + (C\omega)^2}, \quad (\text{B.4})$$

where n_B is the Bose distribution function $n_B(\omega) = 1/(e^{\omega/T} - 1)$ and $K_d = 2\pi^{d/2}/[(2\pi)^d \Gamma(d/2)]$, with Γ being the gamma function. In terms of dimensionless parameters, eqs. (B.3) and (B.4) are rewritten as

$$\mathcal{K}(0) = \frac{T_0 d}{T_A} \int_0^\infty dz' z' \int_0^{x_c} \frac{x^{d+\theta-1} dx}{[x^\theta(y + x^2)]^2 + z'^2}, \quad (\text{B.5})$$

$$\mathcal{K}(T) = \frac{2T_0 d}{T_A} \int_0^\infty \frac{z dz}{e^{2\pi z} - 1} \int_0^{x_c} \frac{x^{d+\theta-1}}{[x^\theta(y + x^2)/t]^2 + z^2}. \quad (\text{B.6})$$

Here, $y = r_0/2T_A = (a_0 + 12cX + 6b\langle\phi\rangle + 12c\langle\phi\rangle^2)/2T_A$, $t = T/T_0$, $T_A = Aq_B^2/2$, and $T_0 = Aq_B^2/2\pi C$, where q_B is the wave vector at the Brillouin zone boundary.

Near the critical end point $y = r_0/2T_A \sim 0$, eq. (B.5) can be expanded in terms of y , and we obtain $\mathcal{K}(0) =$

$K_0 + K_1 r_0$. The z integral in eq. (B·6) can be carried out analytically, and we obtain

$$\mathcal{K}(T) = \frac{T_0 d}{T_A} \int_0^{x_c} dx x^{d+\theta-1} \left[\log u - \frac{1}{2u} - \psi(u) \right], \quad (\text{B} \cdot 7)$$

where ψ is the di-gamma function and $u = x^\theta(y + x^2)/t$. Rescaling x by $t^{1/(2+\theta)}$, eq. (B·7) becomes

$$\mathcal{K}(T) = \frac{T_0 d}{T_A} t^{\frac{d+\theta}{2+\theta}} \int_0^{x_c/t^{\frac{1}{2+\theta}}} ds s^{d+\theta-1} \left[\log u - \frac{1}{2u} - \psi(u) \right]. \quad (\text{B} \cdot 8)$$

Here, $u = \alpha(y, t, \theta) s^\theta + s^{2+\theta}$ with $\alpha(y, t, \theta) = y/t^{\frac{2}{2+\theta}}$. As discussed by Misawa *et al.*,²⁹ eq. (B·8) is proportional to $t^{\frac{d+\theta}{2+\theta}}$ if $\alpha(y, t, \theta) \rightarrow 0$ for $t \rightarrow 0$. This is understood by noting that $u \rightarrow s^{2+\theta}$ for $t \rightarrow 0$ and the integral has no t dependence for a small t .

- 1) F. Steglich, J. Aarts, C. D. Bredl, W. Lieke, D. Meschede, W. Franz, and J. Schäfer: Phys. Rev. Lett. **43** (1979) 1892.
- 2) G. R. Stewart: Rev. Mod. Phys. **73** (2001) 797.
- 3) B. Bellarbi, A. Benoit, D. Jaccard, J. M. Mignot, and H. F. Braun: Phys. Rev. B **30** (1984) 1182.
- 4) E. Vargoz and D. Jaccard: J. Magn. Magn. Mater. **177-181** (1998) 294.
- 5) D. Jaccard, H. Wilhelm, K. Alami-Yadri, and E. Vargoz: Physica B **259-261** (1999) 1.
- 6) H. Yuan, F. M. Grosche, M. Deppe, C. Geibel, G. Sparn, and F. Steglich: Science **302** (2003) 2104.
- 7) A. Holmes, D. Jaccard, and K. Miyake: Phys. Rev. B **69** (2004) 024508.
- 8) K. Fujiwara, Y. Hata, K. Kobayashi, K. Miyoshi, J. Takeuchi, Y. Shimaoka, H. Kotegawa, T. C. Kobayashi, C. Geibel, and F. Steglich: J. Phys. Soc. Jpn. **77** (2008) 123711.
- 9) K. Miyake, T. Matsuura, and C. M. Varma: Solid State Commun. **71** (1989) 1149.
- 10) Y. Onishi and K. Miyake: J. Phys. Soc. Jpn. **69** (2000) 3955.
- 11) S. Watanabe, M. Imada, and K. Miyake: J. Phys. Soc. Jpn. **75**

- (2006) 043710.
- 12) Y. Saiga, T. Sugibayashi, and D. S. Hirashima: J. Phys. Soc. Jpn. **77** (2008) 114710.
- 13) K. Miyake and H. Maebashi: J. Phys. Soc. Jpn. **71** (2002) 1007.
- 14) S. Horn, E. Holland-Moritz, M. Loewenhaupt, F. Steglich, H. Scheuer, A. Benoit, and J. Flouquet: Phys. Rev. B **23** (1981) 3171.
- 15) G. Knopp, J. Spille, A. Loidl, K. Knorr, U. Rauchschwalbe, R. Felten, G. Weber, F. Steglich, and A. P. Murani: J. Magn. Magn. Mater. **63-64** (1987) 88.
- 16) Y. Nishida, A. Tsuruta, and K. Miyake: J. Phys. Soc. Jpn. **75** (2006) 064706.
- 17) H. Miyagawa, G. Oomi, M. Ohashi, I. Satoh, T. Komatsubara, M. Hedo, and Y. Uwatoko: Phys. Rev. B **78** (2008) 064403.
- 18) M. Loewenhaupt, B. D. Rainford, and F. Steglich: Phys. Rev. Lett. **42** (1979) 1709.
- 19) A. Georges, G. Kotliar, W. Krauth, and M. Rozenberg: Rev. Mod. Phys. **68** (1996) 13.
- 20) K. G. Wilson: Rev. Mod. Phys. **47** (1975) 773.
- 21) R. Bulla, T. A. Costi, and T. Pruschke: Rev. Mod. Phys. **80** (2008) 395.
- 22) A. Weichselbaum and J. v. Delft: Phys. Rev. Lett. **99** (2007) 076402.
- 23) R. Peters, T. Pruschke, and F. B. Anders: Phys. Rev. B **74** (2006) 245114.
- 24) T. Moriya and A. Kawabata: J. Phys. Soc. Jpn. **34** (1973) 639.
- 25) T. Moriya and A. Kawabata: J. Phys. Soc. Jpn. **35** (1973) 669.
- 26) T. Moriya: *Spin Fluctuations in Itinerant Electron Magnetism* (Springer-Verlag, Berlin, 1985).
- 27) A. J. Millis, A. J. Schofield, G. G. Lonzarich, and S. A. Grigera: Phys. Rev. Lett. **88** (2002) 217204.
- 28) M. Dzero, M. R. Norman, I. Paul, C. Pépin, and J. Schmalian: Phys. Rev. Lett. **97** (2006) 185701.
- 29) T. Misawa, Y. Yamaji, and M. Imada: J. Phys. Soc. Jpn. **78** (2009) 084707.
- 30) J. J. Binney, N. J. Dowrick, A. J. Fisher, and M. E. J. Newman: *The Theory of Critical Phenomena* (Clarendon Press, Oxford, 1992) p. 164.
- 31) K. Makoshi and T. Moriya: J. Phys. Soc. Jpn. **38** (1975) 10.
- 32) K. Ueda and T. Moriya: J. Phys. Soc. Jpn. **39** (1975) 605.
- 33) K. Miyake: private communications.
- 34) H. Ikeda: J. Phys. Soc. Jpn. **71** (2002) 1126.